HHS Public Access

Author manuscript

Aerosol Sci Technol. Author manuscript; available in PMC 2016 February 02.

Published in final edited form as:

Aerosol Sci Technol. 2014 ; 48(12): 1254–1263. doi:10.1080/02786826.2014.980883.

Size Distribution and Estimated Respiratory Deposition of Total Chromium, Hexavalent Chromium, Manganese, and Nickel in Gas Metal Arc Welding Fume Aerosols

Lorenzo G. Cena, **William P. Chisholm**, **Michael J. Keane**, **Amy Cumpston**, and **Bean T. Chen**

Health Effects Laboratory Division, National Institute for Occupational Safety and Health, Morgantown, West Virginia, USA

Abstract

A laboratory study was conducted to determine the mass of total Cr, Cr(VI), Mn, and Ni in 15 size fractions for mild and stainless steel gas-metal arc welding (GMAW) fumes. Samples were collected using a nano multi orifice uniform deposition impactor (MOUDI) with polyvinyl chloride filters on each stage. The filters were analyzed by inductively coupled plasma mass spectrometry (ICP-MS) and ion chromatography. Limits of detection (LODs) and quantitation (LOQs) were experimentally calculated and percent recoveries were measured from spiked metals in solution and dry, certified welding-fume reference material. The fraction of Cr(VI) in total Cr was estimated by calculating the ratio of Cr(VI) to total Cr mass for each particle size range. Expected, regional deposition of each metal was estimated according to respiratory-deposition models. The weight percent (standard deviation) of Mn in mild steel fumes was 9.2% (6.8%). For stainless steel fumes, the weight percentages were 8.4% (5.4%) for total Cr, 12.2% (6.5%) for Mn, 2.1% (1.5%) for Ni and 0.5% (0.4%) for Cr(VI). All metals presented a fraction between 0.04 and 0.6 μm. Total Cr and Ni presented an additional fraction <0.03 μm. On average 6% of the Cr was found in the Cr(VI) valence state. There was no statistical difference between the smallest and largest mean Cr(VI) to total Cr mass ratio (p-value D 0.19), hence our analysis does not show that particle size affects the contribution of Cr(VI) to total Cr. The predicted total respiratory deposition for the metal particles was ∼25%. The sites of principal deposition were the head airways (7–10%) and the alveolar region (11–14%). Estimated Cr(VI) deposition was highest in the alveolar region (14%).

Introduction

Welding is a common operation in manufacturing that generates a number of hazards. These hazards include fumes, gases, and physical agents such as UV, IR radiation and heat

Address correspondence to Lorenzo G. Cena, Health Effects Laboratory Division, National Institute for Occupational Safety and Health, 1095 Willowdale Road, Morgantown, WV 26508, USA. lcena@cdc.gov.

Disclaimer: The findings and conclusions in this article are those of the authors and do not necessarily represent the views of the National Institute for Occupational Safety and Health. The mention of any company names or products does not imply an endorsement by NIOSH or the Center for Disease Control and Prevention, nor does it imply that alternative products are unavailable, or unable to be substituted after appropriate evaluation.

Supplemental Material: Supplemental data for this article can be accessed on the publisher's website.

(Antonini 2003). Gas-metal arc welding (GMAW) is a commonly used welding process often referred to as metal inert gas or MIG welding that has significantly increased in popularity. A gas-shielded torch is supplied with 100% inert (Ar or He) or more commonly with a combination of inert and active (CO_2, O_2 or other mixtures) gases. The use of Ar mixtures (>75% Ar) in shield gas and the associated increase in voltage allow for increased-quality welds in spray mode, where the electrode wire tip is transferred as a fine spray into the welding pool (Keane et al. 2009). The electrode is a consumable metal wire supplied by a motorized feeder. Fumes generated during this process are composed of metal and metal oxides of iron (Fe), manganese (Mn), nickel (Ni), chromium (Cr), and other volatilized chemical species (Zimmer and Biswas 2001; Keane et al. 2010). The metal vapors generated during the welding process undergo coagulation as they cool in ambient air. This process leads to the formation of chain agglomerates.

The hazards associated with inhalation of welding fumes can be related to the composition of the consumables that melt and are transferred to the welding pool, the welding substrate, and the shield gas type. Published literature states that arc welding fumes primarily come from the electrode wire, however, the fume generation rates are also affected by the welding mode (i.e., axial spray, short circuit, pulsed spray), the welding parameters (voltage and current) and the shield gas type (Castner and Null 1998; Keane et al. 2009). The primary constituents of GMAW fumes generated during mild steel welding are Fe and Mn. Fe is considered a nuisance dust with little likelihood of causing chronic lung disease, while Mn has been associated with neurological diseases (McMillan 1999; Antonini 2003; NIOSH 2007). Welding on stainless steel presents added occupational hazards compared to mild steel due to exposure to hexavalent chromium (Cr(VI)) and Ni, two known carcinogens also associated with asthma (Gibb et al. 2000; Park et al. 2004b; NIOSH 2007).

The particle size distribution of welding fumes has significance to the deposition in the respiratory tract and the level of toxicity. The size of arc welding fume particles ranges between 0.05 and 20 μm (Zimmer and Biswas 2001). Inhaled particles may deposit throughout the respiratory system or they may be exhaled. Several mechanisms affect particle deposition, the most important of which are impaction, settling and diffusion. Particles that contact the airway surfaces deposit there and are not exhaled. Generally as particle size decreases, their ability to penetrate deeper into the respiratory system increases (Görner and Fabriès 1996). However, as particle size decreases, diffusion has a stronger effect and further increases deposition rates in all regions. A fraction of particles smaller than 0.5 μm may also deposit in the upper airways (ICRP 1994). The parameters that determine the extent and location of particle deposition are particle size, density and shape; airway geometry; and the individual's breathing pattern (Hinds 1999). Although many studies have examined fume generation rates of Mn, Cr and Ni for various welding processes, few have specifically investigated the size distribution of each metal.

The majority of the published literature reports bulk metal measurements from filter samples. Castner and Null (1998) measured fume generation rates and total fume (TF) composition of several metals, including Mn, Cr, Cr(VI) and Ni during flux-cored arc welding (FCAW), shielded metal arc welding (SMAW) and GMAW. Kobayashi et al. (1983) reported total Mn content in fumes generated during FCAW. Jenkins and Eagar

(2005) investigated the composition by weight of bulk mild steel GMAW and SMAW fumes. Yoon et al. (2003) investigated concentrations of total Cr and Cr(VI) in fumes generated during FCAW of stainless steel collected on glass fiber and polyvinyl chloride (PVC) filers. Pedersen et al. (1987) measured the content of Cr(VI) vs. total Cr in GMAW of stainless steel collected on PVC and cellulose acetate filters. Antonini (2006) characterized the fume particles generated with a robotic welding-fume generator and reported the bulk metal composition of stainless steel welding fumes.

Other studies looked at metal contents in differentiated size fractions. Keane at al. (2009) sampled fumes in two size ranges, a microspatter fraction (≥0.6 μm) and a fine (<0.6 μm) fraction, which were than analyzed for Cr(VI) content. Chang et al. (2013) analyzed mild steel welding fumes collected using a compact cascade impactor; metal concentrations were reported in three particle size ranges, coarse ($PM_{2.5–10}$), fine ($PM_{0.1–2.5}$) and ultrafine ($PM_{0.1}$). Tandon et al. (1986) used atomic absorption spectroscopy to measure Mn content of high-manganese hardfacing SMAW fumes separated by a cascade impactor. Jenkins (1997) collected GMAW fumes with an Anderson eight-stage cascade impactor. Particles from four stages were transferred to adhesive electron microscopy stubs and metals' content was determined by scanning electron microscopy with energy dispersive spectrometry. Hewett (1995a) measured the particle size distribution for fumes from mild and stainless steel GMAW and SMAW consumables; using a multi orifice uniform deposition impactor (MOUDI) he analyzed particles in ten size fraction for Fe, Mn, Ni and Cr by inductively coupled plasma atomic emission spectroscopy. Subsequently, Hewett (1995b) estimated the regional pulmonary deposition of bulk GMAW and SMAW fumes using mathematical models. These two latter studies provide the best available reconstruction of particle size distributions, however, hexavalent chromium was not evaluated and particle deposition in the head airways was not estimated. Additionally, over the past two decades technology has improved and the concerns for adverse health effects of nanoscale particles have increased. The development of the Nano-MOUDIs has provided the ability to sample smaller particle fractions (as low as 10 nm) with higher resolution.

The objectives of this work were to assess the particle size distribution from nanosize to >30 μm of total Cr, Cr(VI), Mn and Ni in welding fumes generated by GMAW of mild and stainless steel, to establish the fraction of Cr(VI) in total Cr for each particle size range, and to provide an understanding of the regional deposition of these metals in the respiratory system. This understanding has implications for the assessment of hazards to workers who inhale welding fumes.

Methods

Experimental Setup and Sampling

Welding fumes were generated with a six-axis robotic arm welder (Lincoln Electric 100 iB, Cleveland, OH) capable of performing virtually continuous welding lines, described in detail by Antonini et al. (2006). The welder was located inside a walk-in chamber measuring 2.5 m (width) by 3.5 m (depth) by 2.7 m (height) with steady-rate, filtered air supplies. The robotic arm was equipped with a power supply (Lincoln Power Wave 455; Lincoln Electric, Cleveland, OH), a water-cooled arc welding torch (Tregaskiss 450 Amp “Tough Gun”;

Lincoln Electric, Cleveland, OH, USA) and an automatic wire feeder operated at 762 cm (300 inches) per minute. A micro-orifice uniform deposition impactor (MOUDI, Model 10; MSP Corp., Shoreview, MN, USA) and a Nano-MOUDI (Model 115; MSP Corp., Shoreview, MN, USA) were combined and located inside the welding chamber. Particle collection with the combined MOUDI impactors ranged from 0.01 μm to ~32 μm separated in 15 fractions. The MOUDI stages consisted of 47 mm PVC membrane filters (Item No FPVC547; Zefon International, Inc., Ocala, FL, USA). To prevent overloading on certain stages, dilution air was supplied to the MOUDI using an aerosol mixer (In-Tox Products, Moriarty, NM, USA) at 3.33×10^{-4} m^3/s (20 L/min) to provide an aerosol to clean air ratio of 1 to 2.

Four experimental repetitions were conducted for GMAW of T304 stainless steel plates with stainless steel wire (E308LSi; Lincoln Electric, Cleveland, OH, USA) and four repetitions for GMAW of A36 mild steel plates with mild steel wire (ER70S-3; Lincoln Electric, Cleveland, OH). The weight-percent composition of the base materials and electrodes is reported in Table 1. The welder was operated at 25.5 volts and 220 amps with 98% Argon, 2% CO_2 shield gas at 1.13 m^3/hr (40 ft^3/hr) and samples were collected for 40–50 min. Preliminary tests had shown that stages 8–10 of the MOUDI experience the heaviest loading associated with cutpoints ranging from 0.06 μm to 0.18 μm. The welder and MOUDI were paused midway through the sampling and the filters in stages 8–10 were replaced with new PVC filters to ensure collection above the limits of detection (LODs) on the remaining stages while avoiding overload on stages 8–10. Both sets of filters for stages 8–10 were analyzed and the results were added together.

Conventionally, MOUDI samples are collected on aluminum foil substrates and analyzed gravimetrically. Aluminum substrates cannot be easily digested for chemical analysis and plain PVC filters were used as substitutes. The performance of plain PVC filters as collection substrates was tested and compared to greased aluminum substrates (Item No. 0100-96-0573A-X; MSP Corporation, Shoreview, MN, USA) and to greased PVC filters, both sprayed with silicone lubricant (Part No. 07041; MSP Corporation, Shoreview, MN, USA). The comparison was performed with the same stainless-steel-welding sampling conditions. Particle mass distribution, MMAD and GSD for all three substrates were comparable (greased PVC MMAD = 0.25 μm, GSD = 1.5; greased aluminum MMAD = 0.21 μm, GSD = 1.7) to those reported in the “Particle Size Distributions” section below. There was no shift in the distribution of the modes, indicating that the use of PVC filters without grease presented minimal particle bounce in the MOUDI stages. The presence of grease adds several complications to the PVC digestion process, including additional steps and larger dilution volumes which result in larger LODs and limits of quantitation (LOQs). Similar use of plain PVC filters as collection substrate in cascade impactors has been reported by others (Sabty-Daily et al. 2005).

The PVC filters were weighed prior and post sampling in a controlled humidity and temperature environment after an acclimation period of at least 24 h. The electrostatic charges of the filters were neutralized using a U ionizer (PRX-U; HAUG GmbH & Co. KG, Leinfelden-Echterdingen, Germany) and weighing took place on a microbalance with precision to 0.1 μg (XP6U; Mettler Toledo, Columbus, OH, USA). Three method-blank

PVC filters were also weighed prior to each weighing session to account for instrumental fluctuations.

Metal Analysis

Filters from each stage of the MOUDI were split in half, and one half was analyzed by inductively coupled plasma mass spectrometry (ICP-MS) for total Cr, Mn and Ni while the second half was analyzed by ion chromatography (IC) for Cr(VI). The ICP-MS samples were prepared for analysis following NIOSH method 7300 (NIOSH 2003). The following modifications were introduced: (i) to achieve higher temperatures, the hotplate was replaced with a microwave digester (MARS 230/60; CEM Corp, Matthews, NC, USA) with polytetrafluoroethylene vessels and (ii) the digesting acid used was 10 ml of ultra-pure nitric acid which is safer to handle than perchloric acid while achieving the same results. The filters were heated in the microwave digester at 200°C for 30 min and cooled for 20 min. Yttrium certified standard in 2% HNO_3 solution (Claritas PPT Grade Standards; Spex CertiPrep, Metuchen, NJ, USA) was added to each sample as an internal standard. Quality control samples included instrument calibration standards, PVC-filter blanks, and spikes onto filters. The samples were then analyzed by ICP/MS (NexION 300D; PerkinElmer, Toronto, Canada).

The IC samples were prepared by transferring the PVC filters to centrifuge tubes with 10 ml of extraction solution (2% sodium hydroxide, NaOH /3% Sodium carbonate, Na_2CO_3), placing the tubes in ultrasonic bath for 30 min and centrifuging for 15 min at 2400× g. Quality control samples included calibration standards, media blanks, and spikes. The samples were then analyzed by IC (ICS 2500; Dionex Corporation, Sunnyvale, CA, USA).

LOD, LOQ, and Percent Recovery

To determine the LOD and LOQ of the PVC filters we followed two methods, selecting the larger values from each method. For the LOD, the first method consisted of calculating the value three standard deviations above the mean blank signal of fifteen blank PVC filters analyzed for Cr, Ni, and Mn by ICP-MS. The LOQ was calculated as the largest of the mean blank signal plus ten standard deviations and the mass above which recovery was greater than or equal to 75%. The second method consisted in following the standard operating procedure 504 established by NIOSH (2004), and the preparation of six low-level calibration standards, spiked on sampling media, to cover the range from less than the LOD obtained from the media blanks, to no greater than 10 times the media blank's LOD. The low-level calibration standards were analyzed by ICP-MS. The responses on the low-level calibration standards were graphed versus the mass of analyte and the linear regression ($Y = mX + b$) and predicted responses ($\hat{Y}_i$) at each analyte mass (X) were obtained. The standard error of the regression was calculated as $s_y = [\Sigma(\hat{Y}_i - \hat{Y}_i)^2/(N\text{-}2)]^{1/2}$, where N is the number of low-level calibration standards (Neter et al. 1996). The LOD was then calculated as LOD D $3s_y/m$, where m is the slope of the regression line. Subsequently, the LOQ was calculated as LOQ = 3.33 × LOD. Cr(VI) was undetected in the PVC filter blanks. The estimated LOD for method 7605 is 0.02 μg per sample, and the method range is 0.05 to 20 μg of Cr(VI) per sample (NIOSH 2003).

To test the recovery method, three independent replicates of PVC filters were spiked with 1–20 μg of Cr, 0.3–4 μg of Ni or 1–10 μg of Mn standards in 2% HNO_3 (Claritas PPT Grade Standards; Spex CertiPrep, Metuchen, NJ). The Cr(VI) standard was 1–2 μg of $K_2Cr_2O_7$ in water (Product # 2095-4; Ricca Chemical Company, Arlington, TX, USA) spiked on 3 independent replicates of PVC. These amounts were estimated as typical loadings of each metal and were obtained from preliminary runs. Each replicate was analyzed on a separate day with fresh calibration standards. The percent recoveries for each element were then averaged and the standard deviation was calculated. Additionally, the recovery method was tested with three replicates of dry, certified stainless steel welding fume reference material (SSWF-1; The Health and Safety Laboratory, Harpur Hill, Buxton, Derbyshire, UK).

Data Analysis

We calculated the mass percent normalized by stage width (the upper and lower particle-size range of each stage) for total fume (TF) and for each individual metal using a data inversion method (O'Shaughnessy and Raabe 2003). For TF, the mass concentration on each MOUDI stage was obtained from the gravimetric analysis of the PVC filters prior to splitting the samples. The mass concentration of each individual metal was obtained from the ICP-MS and IC analysis of the MOUDI stages. The mass median aerodynamic diameter (MMAD) and the geometric standard deviation (GSD) were calculated on the main mode. The GSD was calculated as the square root of the ratio of the particle size associated with a cumulative count of 84% to that associated with a cumulative count of 16% (Hinds 1999).

The total Cr, Cr(VI), Mn, and Ni content from each MOUDI stage were used to calculate the mass fraction of each metal normalized for interval width. The normalized mass fraction was averaged across the replicates. An upper limit of 32 μm was assumed for computing the mass fraction of the first MOUDI stage (Hinds 1986). The contribution of Cr(VI) relative to total Cr was estimated by calculating the ratio of Cr(VI) mass to total Cr mass for each particle size range of welding fume.

Following Sabty-Daily et al. (2005), the percentage fraction of Cr, Cr(VI), Mn, and Ni deposited in the head airways, tracheobronchial and alveolar regions of the respiratory tract were estimated based on the respiratory deposition model developed by the International Commission on Radiological Protection (ICRP 1994). For each size range of the replicates, we estimated deposition fractions using the midpoint of each MOUDI stage and equations developed by Hinds (1999). These equations are for spheres at standard density; however, diffusion dominates deposition for particles smaller than 0.5 μm. Lung deposition of ultrafine particles is more likely to be determined by particle diffusion (mobility size) than inertia (aerodynamic size) (Park et al. 2008). Scheckman and McMurry (2011) studied the relationship between mobility size and aerodynamic size for silica agglomerates' deposition in a cast of a human lung and found deposition of agglomerates to be significantly greater than that of spheres. Park et al. (2008) showed that for agglomerate soot, aerodynamic diameter is nearly independent of mobility diameter for mobility diameters ranging from 0.1 to 0.8 μm. We expect welding fume agglomerates to behave similarly to other agglomerates; therefore for particles less than 0.5 μm the aerodynamic distributions of the MOUDI were

converted to mobility diameter (d_e). This conversion takes into account particle density and shape as follows,

$$d_e = d_a \left(\frac{C(d_e)}{C(d_a)} \right)^{-1/2} \left(\frac{\rho_p}{\rho_0 \chi} \right)^{-1/2}, \quad [1]$$

where d_a is the midpoint aerodynamic diameter of the MOUDI stages smaller than 0.5 μm, C is the slip correction factor, ρ_p is the effective density, ρ_0 is the standard particle density (1.0 g/cm^3) and χ = 1.68, the dynamic shape factor for chain agglomerates with axial ratio of 10 (Hinds 1999). The major component of welding fume aerosols is iron oxide (FeO) which has density of 5.2 g/cm^3. The effective density of welding fumes has not been investigated in detail; however, effective density of agglomerated particles has been studied for other agglomerated materials and found to differ from the material density (Ahlvik et al. 1998). As particles' size increases, their morphology becomes more irregular and agglomerated thus leading to smaller effective density (Park et al. 2003). Similarly, larger welding fume agglomerates would be expected to have smaller effective density than the density of individual FeO particles. Park et al. (2004a) reported measurements of the inherent material density of different sizes of carbon soot particles and the same group also reported the effective density for agglomerated diesel particles which was smaller and further decreased as the size of the agglomerates increased (Park et al. 2003). We applied a similar approach to estimate the size-dependent effective density of welding fume agglomerates. This was calculated for each particle size by applying the ratio of measured effective density reported in figure 5 of Park et al. (2003) and the density of carbon soot to the density of FeO.

The deposition fraction for the head airways (DF_{HA}) was calculated as

$$DF_{HA} = IF \left(\frac{1}{1+\exp(6.84+1.183\ln d_p)} + \frac{1}{1+\exp(0.924-1.885\ln d_p)} \right), \quad [2]$$

where IF is the inhalable fraction given by

$$IF = 1 - 0.5 \left(1 - \frac{1}{1+0.00076 d_p^{2.8}} \right) \quad [3]$$

and d_p is the midpoint diameter of each of the aerosol size fractions sampled with the MOUDI for particles larger than 0.5 μm and was substituted with d_e for particles smaller than 0.5 μm. The deposition fraction for the tracheobronchial region DF_{TB} is

$$DF_{TB} = \left(\frac{0.00352}{d_p} \right) [+63.9\exp(-0.819(\ln d_p - 1.61)^2)]. \quad [4]$$

The deposition fraction for the alveolar region DF_{AL} is

$$\mathrm{DF}_{\mathrm{AL}}=\left(\frac{0.0155}{d_p}\right)\left[\exp(-0.416(\ln d_p+2.84)^2)+19.11\exp(-0.482(\ln_{dp}-1.362)^2)\right]. \quad [5]$$

The total deposition DF is

$$\mathrm{DF}=\mathrm{IF}\left(0.0587+\frac{0.911}{1+\exp(4.77+1.485\ln d_p)}+\frac{0.943}{1+\exp(0.508-2.58\ln d_p)}\right). \quad [6]$$

For each experimental run and each metal, the estimated percentage of total aerosol deposited in the head airways ($\mathrm{Metal}_{\mathrm{HA}}$) was calculated as

$$\mathrm{Metal}_{\mathrm{HA}}=\frac{\sum_{i=1}^{15}\mathrm{Metal}_{\mathrm{M}i}\times\mathrm{DF}_{\mathrm{HA}i}}{\sum_{i=1}^{15}\mathrm{Metal}_{\mathrm{M}i}}\times 100\%, \quad [7]$$

where $\mathrm{Metal}_{\mathrm{M}i}$ is the mass obtained for each metal from each MOUDI stage *i*. The percentages were then averaged across all four replicates. Similarly, depositions in the other respiratory regions were calculated using the appropriate deposition fraction (Equations (4)–(6)).

Results and Discussion

LOD, LOQ, and Percent Recovery

The results of the LOD and LOQ calculations for PVC filters are reported in Table 2. With the exception of Mn, the LODs and LOQs obtained from the filter blanks and the low-level spikes were comparable. Slightly greater values corresponded with the LODs and LOQs obtained from filter blanks (Table 2). The percent recovery was greater than 90% for all 6 low-level spike amounts. For the gravimetric analysis, the LOD obtained from the standard deviation of several filter blanks was 21.2 μg while the LOQ was 70.6 μg.

Recovery was evaluated over a range of filter loadings for both metals in solution and solid certified welding-fume reference material. The average percent recoveries of the metal spikes in solution and the average recovery of solid welding-fume particles using certified stainless-steel welding-fume reference material are reported in Table 2 along with standard deviation estimates. All recoveries were above 95%.

Particle Size Distributions

The mass percentages normalized per stage width for the TF mass of mild steel obtained from gravimetric analysis of the PVC filters is shown in Figure 1. Similar results were obtained for stainless steel welding, with both welding types presenting tri-modal distributions. The error bars in Figure 1 represent the standard error of the four replicate tests. The most significant mass contribution was found in the size range with cut-off diameters 0.1–1.0 μm. A significant mass contribution was also found in the particle's range 0.01–0.1 μm. A third mode was observed in the particles larger than 3 μm. The MMADs and GSDs of the primary modes for TF and for each metal analyzed are reported in Table 3. For

mild steel welding, the MMAD of the average TF mass was 0.23 μm (GSD D 1.7). Similarly, the MMAD of the stainless steel TF mass was 0.25 μm (GSD D 1.8). The MMADs for each metal fell between 0.19 and 0.26 μm, consistent with the primary mode of the TF mass. As shown in Table 3, the GSDs were also comparable.

The type of welding process and the welding consumables have been found to affect the generated fumes. Previous work from Antonini et al. (2006) reported that the particle morphology, size, and chemical composition of the welding fumes generated with this robotic system are comparable to welding fumes observed and studied by other investigators and are representative of fumes that workers may be exposed to.

The amounts of each metal in the fumes, calculated as percentages of the total welding fume mass, are reported in Table 3. Mn concentrations were 9.2% in mild steel welding fumes and 12% in stainless steel welding fumes. Others have reported manganese concentrations in steel welding fumes between 1 and 15% (wt-%) of the total fume (Kobayashi et al. 1983; Tandon et al. 1986; Castner and Null 1998; Jenkins and Eagar 2005). Ni and Cr in our mild steel welding fumes were below the limit of detection. For stainless steel fumes, Ni was 2.1%, total Cr was 8.4%, and Cr(VI) was 0.5% (Table 3). Castner and Null (1998) reported that the composition of GMAW fumes generated from welds of three different steel plates (A-36, HY-100, and HSLA-100) were virtually identical, with <0.2% of total Cr, <0.1% of Cr(VI) and 1% of Ni in the fumes in spite of different Cr and Ni content of the steel plates. They concluded that the arc welding fumes' particles primarily came from the MIL-100S-1 alloy steel electrode wire, with reported Cr content of 0.1–0.3% and 1.4% of Ni, and not from the plates.

Although the metal content of the fumes was expected to reflect to a certain extent the composition of the welding wire and the steel plates, they did not appear to be directly correlated. The discrepancy is particularly apparent with stainless steel. Ni content in the stainless steel base material and electrodes was ∼10% (Table 1) while only 2% of the fumes contained Ni (Table 3). The stainless steel base metal and electrode contain ∼2% Mn, an order of magnitude lower than the ∼20% of Cr (Table 1). Conversely, the mass concentration measured by the MOUDI in the fumes for Mn (12%, Table 3) was higher than that of Cr (8.4%, Table 3). Others have observed similar Mn enrichment in the fumes (Jenkins 1997; Keane et al. 2010; Cena et al. 2014); Keane et al. (2010) found that the extent of the enrichment is process dependent. In our experiments, Mn enrichment was observed for both types of steel: the reported wt-% of Mn is ∼1% for mild steel plates and wire while the Mn content in the mild steel welding fumes was 9.2%. This phenomenon is not fully understood; Jenkins (1997) discussed possible pathways and suggested that multiple mechanisms may be responsible for Mn enrichment.

A summary of the average mass concentration and percentage of total concentration of Mn, total Cr, Ni, and Cr(VI) in specified size ranges (obtained from the MOUDI cut-points rounded to the nearest significant digit) can be found in the online supplemental information. The mass of these metals consisted primarily of particles between 0.1 and 0.6 μm. Particles in these size ranges represented 11.3–38.3% of the Mn mass in mild steel welding, and 14.2–47.6% of the Cr mass, 13.8–43.5% of the Mn mass, 16.1–50.5% of the

Ni mass and 11.9–47.9% of the Cr(VI) mass in stainless steel welding. Similarly, Chang et al. (2013) and Jenkins (1997) reported that for mild steel GMAW fumes collected with a cascade impactor, these metals were found in higher concentrations in the fine particle fraction that forms from vapor and not in the coarse particles that form from liquid. The normalized mass fraction/μm of each metal under investigation is depicted in Figure 2. Figure 2a shows that Mn mass in mild steel welding has a submicron fraction between 0.04 and 0.6 μm and a unimodal distribution. Figure 2b shows that total Cr and Ni mass in stainless steel welding have a submicron fraction between 0.04 and 0.6 μm but also a fraction <0.03 μm, indicating a multi-modal size distribution. Cr(VI) and Mn in stainless steel welding have a submicron fraction between 0.04 and 0.6 μm and a unimodal distribution. Hewett (1995a) reported a larger distribution for Mn, Ni, and Cr generated during mild and stainless steel GMAW: the distribution of each metal was unimodal and matched the total fume distribution spanning between 0.1 μm and 1 μm. The experimental setup used by Hewett (1995a), however, included a secondary sampling plenum which may have promoted particle agglomeration, did not include the nano MOUDI stages which collect particles as small as 0.01 um, and used 100% argon as shield gas. The combination of 98% argon and 2% CO_2 used in our setup is more prominently used among welders. Keane et al. (2009) and Yoon et al. (2003) found that metal concentrations vary significantly with different welding parameters, including the shield gas type. These parameters may also affect the size distribution of the metals. Our results for hexavalent chromium are in line with the findings of Keane et al. (2009) who found in similar welding conditions that Cr(VI) is primarily associated with particles <0.6 μm. Kura (1998) reports that Cr(VI) concentrations for GMAW performed on stainless steel were predominant in the fine particle size range (<0.52 um) where they accounted for 80% of the Cr(VI) concentrations.

Cr(VI) to Total Cr Mass Ratio

Our analysis of Cr(VI) mass and total Cr mass ratios between different particle size ranges of welding fume samples does not show that particle size affects the contribution of Cr(VI) relative to total Cr in stainless steel welding fumes. The ratio of Cr(VI) to total Cr for each particle size fraction averaged across samples is shown in Figure 3. The average mass ratio of Cr(VI) to total Cr in different size fractions ranged from 0.05 (±0.04) to 0.15 (±0.13). There was no statistically significant difference between the smallest and largest mean Cr(VI) to total Cr mass ratios (p-value = 0.19).

In any given size range, less than 20% of the chromium was in the Cr(VI) valence state. Overall, the average mass percentage of Cr(VI) was 0.5% (±0.4%) while that of total Cr was 8.4% (±5.4), indicating that on average 6% of the Cr in the welding fume was in the Cr(VI) valence state. Others have reported hexavalent chromium concentrations from GMAW processes, ranging between 0.2 and 1% and that 3.5% of the Cr in GMAW welding was in the Cr(VI) valence state in dry filter samples (Pedersen et al. 1987; Voitkevich 1995).

Respiratory Deposition of Metal Aerosols

The mean percentages of metal aerosol estimated to deposit in the head airways, tracheobronchial and alveolar regions of the respiratory system are presented in Table 4. The estimated percentages of metal aerosols in the respiratory sites were calculated based on the

mass distributions measured with the MOUDI. The potential sites of major deposition of the metals under investigation were the head airways and the alveolar region. As shown in Figure 2, the majority of the mass of Cr, Mn, and Ni is contained in the size fractions between 0.1 and 0.6 μm. This size fraction consists mostly of particles that are too large to effectively deposit in the respiratory system by diffusion mechanisms, and too small for impaction or interception to be effective (Hinds 1999). The predicted total deposition for light work, nose breathing based on the ICRP deposition model (ICRP 1994) for particles in this size range is about 20%. Our approximation of welding fume particles' deposition considers the effect of particle shape and density as they have been found to significantly affect respiratory deposition for agglomerates (Scheckman and McMurry 2011).

The least likely site for deposition of the metal fumes' aerosol was the tracheobronchial region where only ∼6% of the total fumes and 2–3% of the individual metal aerosols' mass was estimated to potentially deposit. Total deposition was estimated to 23–27% for the individual metal aerosols and ∼40% for the total fumes of both steel types. Regional deposition of metal particles may affect their absorption, uptake into cells, removal mechanism and ultimately their toxicity (Graham et al. 2010). Cr(VI) is a potential carcinogen; this study found that for Cr(VI) the estimated deposition of sampled stainless steel welding fumes was highest in the alveolar region (Table 4, 14%).

Hewett (1995b) estimated regional pulmonary deposition (tracheobronchial and alveolar) for GMAW total fumes and predicted 40% deposition for both mild and stainless steel consumables with the majority of the particles (31%) depositing in the alveolar region. Our estimations for total fumes' deposition indicate similar deposition for mild and stainless steel (Table 4). Our work also indicates the alveoli as the size of largest deposition although at about half of the magnitude estimated by Hewett. The differences with the experimental setup used by Hewett were described above and the smaller particle size distributions measured in our work may explain the discrepancy between the estimated depositions. As particle size decreases, diffusion has a stronger effect and increases deposition rates in the upper airways. Additionally, the regional deposition functions used by Hewett come from empirical pulmonary deposition model described by Stahlhofen et al. (1989) which have some discrepancies with the ICRP model. The estimated alveolar deposition described by Hewett is congruent with deposition models which indicate that alveolar deposition is greater than tracheobronchial deposition in all particles sizes between 0.01 and 1 μm.

Conclusions

The mass of total Cr, Mn, Ni, and Cr(VI) in mild and stainless steel welding fumes generated in a laboratory setting consisted primarily of particles between 0.04 and 0.6 μm. Total fume mass obtained from gravimetric analysis of MOUDI stages presented a tri-modal distribution with a substantial contribution of particles in the 0.006–0.06 μm range. Chemical analysis of individual metals did not reveal as prominent mass in this smaller size range. The smallest mode may be a result of a different particle formation mechanism or particles that were not detected in the chemical analysis. Six percent of the Cr was found in the Cr(VI) valence state and particle size did not appear to affect the Cr(VI) to total Cr ratio with statistical significance. The metal composition of the welding fumes differed from the

composition of the welding wire. About 25% of the metals under investigation if inhaled by a welder may deposit in the respiratory system. The sites of principal deposition were the head airways and the alveolar region. Hexavalent chromium deposition was highest in the alveolar region (14%) compared to other regions of the respiratory system. Future research should focus on other welding processes such as SMAW, FCAW, and gas tungsten arc welding. Future work should investigate in more detail the relationship between welding parameters, consumables and fumes' composition. Furthermore, the health effects of particular constituents of welding fumes should be investigated.

Supplementary Material

Refer to Web version on PubMed Central for supplementary material.

References

Ahlvik P, Ntziachristos L, Keskinen J, Virtanen A. Real Time Measurements of Diesel Particle Size Distribution with an Electrical Low Pressure Impactor. SAE Tech Pap, No 980410. 1998

Antonini JM. Health Effects of Welding. Crit Rev Toxicol. 2003; 33:61–103. [PubMed: 12585507]

Antonini JM, Afshari AA, Stone S, Chen B, Schwegler-Berry D, et al. Design, Construction, and Characterization of a Novel Robotic Welding Fume Generator and Inhalation Exposure System for Laboratory Animals. J Occup Environ Hyg. 2006; 3:194–203. [PubMed: 16531292]

Castner H, Null C. Chromium, Nickel and Manganese in Shipyard Welding Fumes. Weld J. 1998; 77:223–231.

Cena L, Keane MJ, Chisholm WP, Stone S, Harper M, et al. A Novel Method for Assessing Respiratory Deposition of Welding Fume Nanoparticles. J Occup Environ Hyg. 201410.1080/15459624.2014.91939

Chang C, Demokritou P, Shafer M, Christiani D. Physico-chemical and Toxicological Characteristics of Welding Fume Derived Particles Generated from Real Time Welding Processes. Environ Sci: Processes Impacts. 2013; 15:214–224.

Gibb HJ, Lees PS, Pinsky PF, Rooney BC. Lung Cancer Among Workers in Chromium Chemical Production. Am J Ind Med. 2000; 38:115–126. [PubMed: 10893504]

Görner P, Fabriès JF. Industrial Aerosol Measurement According to the New Sampling Conventions. Occupat Hyg. 1996; 3:361–376.

Graham, JA.; Gardner, DE.; Gardner, SCM.; Miller, FJ. Toxicity of Airborne Metals. In: McQueen, CA., editor. Comprehensive Toxicology. 2nd. Elsevier; Oxford: 2010.

Hewett P. The Particle Size Distribution, Density, and Specific Surface Area of Welding Fumes from SMAW and GMAW Mild and Stainless Steel Consumables. Am Ind Hyg Assoc J. 1995a; 52:128–135. [PubMed: 7856513]

Hewett P. Estimation of Regional Pulmonary Deposition and Exposure for Fumes from SMAW and GMAW Mild and Stainless Steel Consumables. Am Ind Hyg Assoc J. 1995b; 56:136–142. [PubMed: 7856514]

Hinds, WC. Data Analysis. In: Lodge, J.; Chan, T., editors. Cascade Impactor: Sampling and Data Analysis. American Industrial Hygiene Association; Akron, OH: 1986.

Hinds, WC. Aerosol Technology, Properties, Behavior, and Measurement of Aerosol Particles. John Wiley & Sons Inc; New York, NY: 1999.

ICRP. Human Respiratory Tract Model for Radiological Protection. 1994 Publication 66.

Jenkins, NT. Chemistry of Airborne Particles from Metallurgical Processing. Doctoral Dissertation; Massachusetts Institute of Technology: 1997.

Jenkins NT, Eagar TW. Chemcial Analysis of Welding Fume Particles. Suppl Weld J. 2005; 84(6):87–93.

Keane M, Stone S, Chen B. Welding Fumes from Stainless Steel Gas Metal Arc Processes Contain Multiple Manganese Chemical Species. J Environ Monit. 2010; 12:1133–1140. [PubMed: 21491680]

Keane M, Stone S, Chen B, Slaven J, Schwegler-Berry D, Antonini J. Hexavalent Chromium Content in Stainless Steel Welding Fumes is Dependent on the Welding Process and Shield Gas Type. J Environ Monit. 2009; 1:418–424. [PubMed: 19212602]

Kobayashi M, Maki S, Hashimoto Y, Suga T. Investigations on Chemical Composition of Welding Fumes. Welding J. 1983; 62:190–196.

Kura, B. Evaluation of Cr(VI) Exposure Levels in the Shipbuilding Industry, GCRMTC Project No 32 ONR Cooperative Agreement No N00014-94-0011. Gulf Coast Region Maritime Technology Center; University of New Orleans: 1998. 1998

McMillan DE. A Brief History of the Neurobehavioral Toxicity of Manganese: Some Unanswered Questions. Neuro Toxicolo. 1999; 20:499–507.

NIOSH. NIOSH Manual of Analytical Methods. U.S. Government Printing Office; Washington, D.C: 2003.

NIOSH. [Accessed 23 July 2013] 2004. http://dart.cdc.gov/lims/labsup/sop/sop504.htm

NIOSH. NIOSH Pocket Guide to Chemical Hazards. U.S. Government Printing Office; Pittsburgh, PA: 2007.

Neter, J.; Kutner, MH.; Nachtsheim, CJ.; Wasserman, W. Applied Linear Statistical Models. Irwin; Chicago: 1996.

O'Shaughnessy PT, Raabe OG. A Comparison of Cascade Impactor Data Reduction Methods. Aerosol Sci Technol. 2003; 37:187–200.

Park K, Cao F, Kittelson DB, McMurry PH. Relationship Between Particle Mass and Mobility for Diesel Exhaust Particles. Environ Sci Technol. 2003; 37:577–583. [PubMed: 12630475]

Park K, Dutcher D, Emery M, Pagels J, Sakurai H, et al. Tandem Measurements of Aerosol Properties—A Review of Mobility Techniques with Extensions. Aerosol Sci Technol. 2008; 42:801–816.

Park K, Kittelson DB, Zachariah MR, McMurry PH. Measurement of Inherent Material Density of Nanoparticle Agglomerates. J Nanopart Res. 2004a; 6:267–272.

Park RM, Bena JF, Stayner LT, Smith RJ, Gibb HJ, Lees PSJ. Hexavalent Chromium and Lung Cancer in the Chromate Industry: A Quantitative Risk Assessment. Risk Anal. 2004b; 24:1099–1108. [PubMed: 15563281]

Pedersen B, Thomsen E, Stern R. Some Problems in Sampling, Analysis and Evaluation of Welding Fumes Containing Cr (VI). Annal Occup Hyg. 1987; 31:325–338.

Sabty-Daily RA, Harris PA, Hinds WC, Froines JR. Size Distribution and Speciation of Chromium in Paint Spray Aerosol at an Aerospace Facility. Ann Occup Hyg. 2005; 49:47–59. [PubMed: 15591325]

Scheckman JH, McMurry PH. Deposition of Silica Agglomerates in a Cast of Human Lung Airways: Enhancement Relative to Spheres of Equal Mobility and Aerodynamic Diameter. J Aerosol Sci. 2011; 42:508–516.

Stahlhofen W, Rudolf G, James A. Intercomparison of Experimental Regional Aerosol Deposition Data. J Aerosol Med. 1989; 2:285–308.

Tandon R, Ellis J, Crisp P, Baker R, Chenhall B. Chemical Investigation of Welding Fumes from Hardfacing and HSLA-Steel Electrodes. Weld J. 1986; 65:231–236.

Voitkevich, V. Welding Fumes: Formation, Properties and Biological Effects. Abington Publishing; Cambridge, England: 1995.

Yoon CS, Paik NW, Kim JH. Fume Generation and Content of Total Chromium and Hexavalent Chromium in Flux-Cored arc Welding. Ann Occup Hyg. 2003; 47:671–680. [PubMed: 14602674]

Zimmer AT, Biswas P. Characterization of The Aerosols Resulting from Arc Welding Processes. J Aerosol Sci. 2001; 32:993–1008.

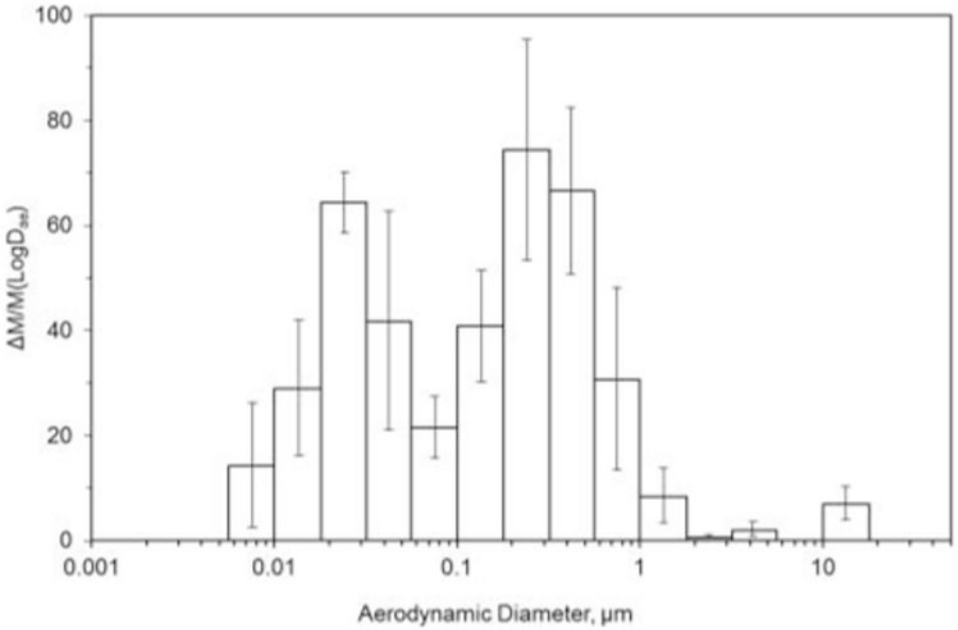

Fig. 1.

Particle size distribution of mild steel gas metal arc welding fume comparing total fume mass versus particle size as measured with the MOUDI and nano-MOUDI impactor system.

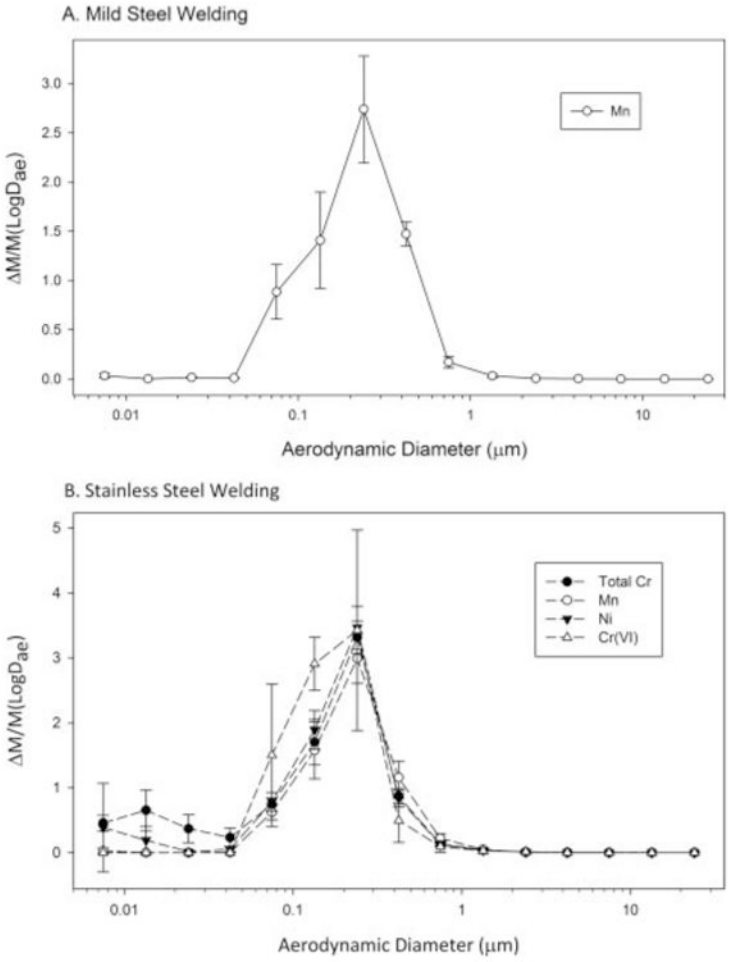

Fig. 2.
Particle size distribution of metals in (a) mild steel and (b) stainless steel welding.

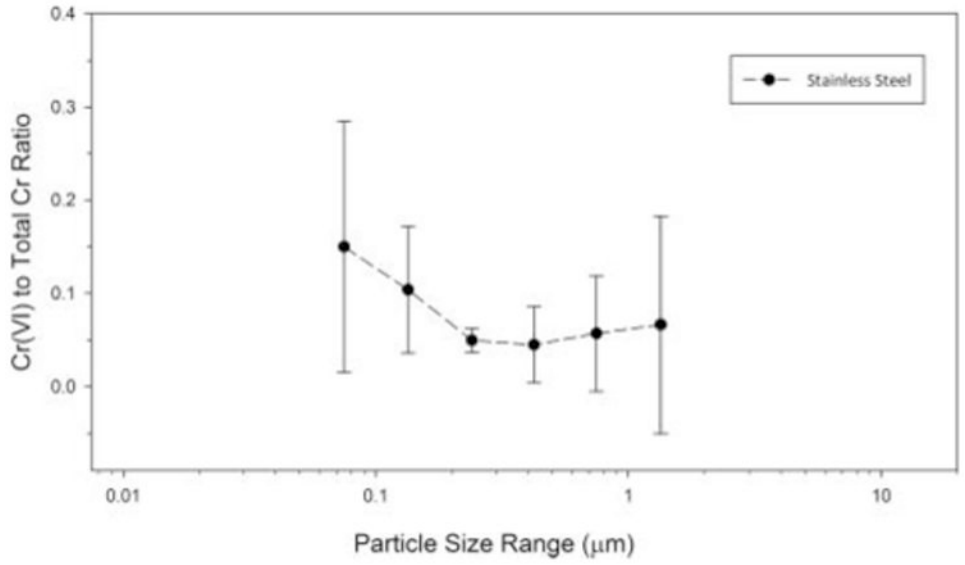

Fig. 3.

Cr(VI) to total Cr ratio by particle size in stainless steel welding (vertical bars represent one standard deviation around the mean).

Table 1

Wt-% composition of base materials and electrodes

Element	A36 mild steel	ER70S-3 wire	T304 stainless steel	308LSi wire
Mn	0.7	1.2	2.0	1.8
Cr	0.06	0.05	18.0	20.8
Ni	0.1	0.04	8.0	9.8

Table 2

Limits of detection (LOD), quantitation (LOQ), and average % recovery ± standard deviation for Cr, Ni, and Mn using ICP-MS, and Cr(VI) using IC

PVC Filters						
Element	**Blanks LOD [*μ*g/filter]**	**Blanks LOQ [*μ*g/filter]**	**Low-level LOD *μ*g/filter]**	**Low-level LOQ [*μ*g/filter]**	**Spikes in solution recovery**	**Certified material recovery**
Cr	0.9	2.99	0.9	2.85	98% ± 2%	96% ± 2%
Mn	0.3	0.95	0.1	0.43	99% ± 3%	99% ± 4%
Ni	0.3	1.11	0.3	1.04	95% ± 6%	99% ± 4%
Cr(VI)	*	*	0.02	0.06	98% ± 8%	n.a.**

* Undetected.

** Not available.

Table 3

MMAD and GSD of the primary mode and wt-% metal content (SD) of all modes for mild and stainless steel welding

	MMAD, μm	GSD	Fumes' metal content, mean (SD),%
Mild Steel			
TF	0.23	1.70	—
Mn	0.26	1.62	9.2 (6.8)
Stainless Steel			
TF	0.25	1.80	—
Mn	0.26	1.63	12 (6.5)
Total Cr	0.22	1.49	8.4 (5.4)
vNi	0.22	1.42	2.1 (1.5)
Cr(VI)	0.19	1.41	0.5 (0.4)

Table 4

Estimated mean percentage (SD) of total aerosol deposited in the head airways, and tracheobronchial and alveolar regions

	Head airways	Tracheobronchial region	Alveolar region	Total
Mild Steel				
TF	12 (2.9)	6.3 (1.2)	17 (3.4)	38 (6.1)
Mn	7.8 (1.1)	2.0 (0.3)	11 (0.9)	23 (1.6)
Stainless Steel				
TF	21 (7.6)	6.5 (4.5)	14 (4.0)	43 (12)
Total Cr	9.6 (1.6)	2.5 (0.2)	11 (0.5)	26 (1.4)
Mn	8.0 (1.1)	1.9 (0.2)	11 (0.7)	23 (1.0)
Ni	8.7 (3.0)	2.2 (0.2)	11 (0.6)	25 (2.1)
Cr(VI)	6.5 (4.6)	3.1 (1.3)	14 (3.0)	27 (6.1)